RSC Advances

PAPER

View Article Online
View Journal | View Issue

Cite this: *RSC Adv.*, 2026, **16**, 14070

A facile and green approach for the surface coating of phosphorus–silicon functionalized graphene oxide to improve flame retardancy of polyurethane foam

Taweesak Boonsod,[a] Qamber Ali,[bc] Kanoktip Boonkerd*[bc] and Wirunya Keawwattana *[ad]

Polyurethane foam (PUF) is the most widely used polymeric foam due to its excellent thermal insulation properties, low cost, and low density. However, its applications are limited by fire performance concerns and associated safety issues. This study describes the synthesis of a novel flame retardant and an environmentally friendly coating method aimed at enhancing the fire safety and mechanical integrity of PUF using a water-based polyethyleneimine (PEI) binder. A phosphorus/silicon-containing functionalized graphene oxide (FGO) was successfully synthesized by grafting graphene oxide (GO) with 9,10-dihydro-9-oxa-10-phosphaphenanthrene-10-oxide (DOPO) and 3-glycidoxypropyltrimethoxysilane (GPTMS). The chemical structure of FGO was confirmed by XPS, FTIR, and Raman spectroscopy. FGO and GO were subsequently coated onto PUF surfaces *via* a layer-by-layer assembly method. Combustion tests of the PUF/FGO (5 wt%) revealed a Limiting Oxygen Index (LOI) of 34.2% and a V-0 rating in the UL-94 test. Furthermore, real-time TGA-FTIR analysis demonstrated a 46% reduction in CO_2 evolution and a high char residue of 52%, indicating significant suppression of volatile fuel and smoke hazards. This fire protection is attributed to the formation of a dense phosphosilicate protective layer, which provides a robust barrier effect in both gas and condensed phases. Additionally, the coating treatment remarkably enhanced the mechanical performance of the foam. The compressive strength of PUF/FGO increased by 152% (1.34 MPa) compared to pristine PUF, as the FGO effectively infiltrated structural defects and reinforced the cellular framework. Consequently, FGO demonstrates superior efficacy over GO in providing a multifunctional solution for high-performance, fire-safe PUF.

Received 6th January 2026
Accepted 9th March 2026

DOI: 10.1039/d6ra00124f

rsc.li/rsc-advances

1 Introduction

Various materials have been used in the construction of walls and ceilings in buildings. Among them, polyurethane foam (PUF) has attracted considerable attention due to its advantageous properties, including low density, low thermal conductivity, low moisture permeability, and low water absorption.[1–3] These characteristics make PUF widely used in construction and industrial applications. However, PUF is highly flammable and can ignite rapidly, leading to continuous dripping, fast flame spread, the release of toxic gases, and significant heat generation during combustion.[4,5] These hazards greatly increase fire risk, posing serious threats to both life and property. Consequently, the inherent flammability of PUF remains a major limitation for its practical applications. Therefore, improving the fire resistance of PUF is of critical importance for its safe use in building and construction materials.

Graphene, a two-dimensional nanomaterial widely regarded as one of the "wonder materials" of the 21st century, has attracted considerable research interest due to its exceptional physicochemical properties. These remarkable characteristics enable its utilization in diverse applications, including solar cells, electronics, sensors, biomedical technologies, and composite materials.[6–10] Among graphene-based materials, graphene oxide (GO) has been extensively studied because its oxygen-containing functional groups—such as epoxy, hydroxyl, and carboxyl groups located on the basal plane and edges of the graphene sheets—improve its dispersibility and enable further chemical functionalization.[11] GO can enhance the flame retardancy of polymers through several mechanisms, including the formation of a continuous and dense char layer during thermal decomposition and its large specific surface area,

[a]*Department of Chemistry, Faculty of Science, Kasetsart University, 50 Ngamwongwan Road, Lat Yao, Chatuchak, Bangkok, 10900, Thailand. E-mail: fsciwyk@ku.ac.th*
[b]*Department of Materials Science, Faculty of Science, Chulalongkorn University, 254 Phayathai Road, Bangkok, 10330, Thailand. E-mail: kanoktip.b@chula.ac.th*
[c]*Center of Excellence in Green Materials for Industrial Application, 254 Phayathai Road, Bangkok 10330, Thailand*
[d]*Specialized Center of Rubber and Polymer Materials in Agriculture and Industry (RPM), Faculty of Science, Kasetsart University, Bangkok, Thailand*

which contributes to an effective physical barrier that restricts heat transfer and the diffusion of combustible gases and oxygen.[12–18] However, GO still faces several challenges in the development of graphene-based flame retardants. Its poor dispersion in polymer matrices and strong tendency to agglomerate, caused by π–π interactions and van der Waals forces, limit its effectiveness when used as a standalone flame retardant. Moreover, GO alone generally exhibits insufficient flame-retardant efficiency, making it difficult to achieve the desired level of fire resistance without further modification or combination with other flame-retardant components.[19–21] These limitations can be addressed by grafting additional flame-retardant species onto the surface of GO, as GO possesses abundant reactive oxygen-containing functional groups that provide active sites for chemical grafting, enabling the incorporation of additional flame retardants and thereby enhancing their overall effectiveness.

9,10-Dihydro-9-oxa-10-phosphaphenanthrene-10-oxide (DOPO) is an important phosphorus-based flame retardant due to its excellent environmental compatibility, high thermal stability, and outstanding flame-retardant performance.[22–26] DOPO can function as a flame retardant in both the gas and condensed phases.[27,28] The molecular structure of DOPO contains a reactive P–H bond, which can participate in addition reactions with various functional groups, such as epoxides. However, grafting DOPO directly onto the surface of GO remains challenging because of the limited chemical reactivity between the functional groups of DOPO and those present on the GO surface, leading to low covalent-bonding efficiency. To address this issue, several studies have explored strategies to bridge DOPO with other components through intermediate coupling structures. For example, Liu *et al.* successfully grafted DOPO onto magnesium hydroxide using a vinyl silane coupling agent (MH-WD70-DOPO) and subsequently incorporated it into ethylene–vinyl acetate copolymer (EVA).[29] Wu *et al.* developed epoxy hybrid resins by curing bisphenol A-type epoxy and 4,4′-diaminodiphenylmethane through a sol-gel reaction using phosphorus-containing trimethoxysilane (DOPO–GPTMS).[30] In addition, Chernyy *et al.* prepared flame-retardant materials *via* hydrolysis and condensation reactions involving tetraethoxysilane (TEOS) and a DOPO-based silane derivative (DOPO-VTS).[31]

3-Glycidoxypropyltrimethoxysilane (GPTMS) is a bifunctional silane coupling agent containing both epoxy and Si–O functional groups.[32] Owing to this dual functionality, GPTMS can potentially act as a molecular bridge to link DOPO with GO. In principle, the epoxy groups of GPTMS can react with the reactive P–H bond of DOPO,[33] while the Si–O groups may interact with the oxygen-containing functional groups on the GO surface to form Si–O–C linkages.[34] In addition, the silicon atoms present in the silane structure may further contribute to flame retardancy in polymer systems. Although the synthesis of DOPO-silane compounds has been widely explored for flame-retardant applications, the use of GPTMS as molecular bridges to covalently graft DOPO onto GO for flame-retardant coatings has been rarely reported.

Two common strategies have been developed to reduce the flammability of polymers. One approach involves incorporating flame retardants into polymer matrices, which has been widely used to enhance the flame resistance of polymer materials. However, a relatively large amount of flame retardants is often required to achieve the desired level of flame resistance, which may adversely affect the mechanical properties of polymers, such as tensile and flexural strength.[4] Another strategy involves applying flame-retardant coatings onto the surface of polymers, providing an alternative approach to improving flame retardancy. Among these techniques, the Layer-by-Layer (LbL) self-assembly method has attracted considerable attention due to its unique advantages. Flame-retardant multilayer films constructed by LbL assembly can effectively inhibit combustionby forming a protective barrier between the outer environment and the polymer substrate.[35] In addition, the LbL assembly process is typically carried out under mild experimental conditions, such as room temperature, atmospheric pressure, and low concentrations of building blocks.[36] Owing to these advantages, the LbL assembly method is considered an efficient and cost-effective strategy for fabricating flame-retardant coatings.[37]

Polyethyleneimine (PEI) is a synthetic cationic polymer that can exist in either linear or branched structures and contains primary, secondary, and tertiary amino groups. Owing to its high-water solubility and high nitrogen content, PEI has attracted considerable interest in various applications.[38,39] Depending on the pH of the solution, some of the amino groups can be protonated to form ammonium ions, which impart a strong cationic character to the polymer. As a result, PEI has been widely used in fields such as flame retardancy, water treatment, carbon dioxide capture, and cosmetics.[37]

PEI is frequently employed as a binder or polyelectrolyte in LbL assembly systems for constructing flame-retardant coatings. Several studies have reported the fabrication of flame-retardant multilayer coatings on flexible polyurethane foam (FPUF) using PEI-based LbL assembly. For instance, Pan *et al.* deposited graphene-based multilayer films on FPUF through alternate immersion in sodium alginate/GO suspensions and PEI solution.[40] In another study, graphene oxide and amino-terminated silica nanospheres were assembled into hybrid flame-retardant coatings *via* the LbL technique.[41] Similarly, Shi *et al.* constructed multilayer coatings composed of PEI, GO, and synthetic melanin nanoparticles on PUF.[42] Other studies have also reported PEI-based LbL coatings incorporating PDA-rGO, phytic acid, alginate, and sepiolite to enhance the flame retardancy of FPUF.[43–45]

Based on the above concept, the main objective of this study was to synthesize a novel phosphorus-silicon-containing graphene-based flame retardant, hereafter referred to as functionalized graphene oxide (FGO), by covalently grafting GO with a DOPO-GPTMS adduct. The synthesized FGO was subsequently deposited onto polyurethane foam (PUF) using an environmentally friendly LbL assembly technique. In this process, PEI was employed as a binder to construct multilayer coatings. The entire coating procedure was carried out in an aqueous system using deionized water as the sole solvent at room temperature, providing a simple, green, and highly controllable strategy for

fabricating flame-retardant coatings. This LbL approach enables efficient deposition of functionalized graphene oxide while achieving significant improvement in fire resistance with only a limited number of coating layers. The chemical structure of the synthesized FGO, together with the thermal degradation behavior and fire performance of the coated PUF samples, was systematically investigated.

2 Experimental

2.1 Raw materials

Graphite powder was purchased from Sigma-Aldrich Co., Ltd. 9,10-Dihydro-9-oxa-10-phosphaphenanthrene-10-oxide (DOPO) was obtained from Tokyo Chemical Industry Co., Ltd. 3-Glycidoxypropyltrimethoxysilane (GPTMS) was supplied by Thermo Fisher Scientific Inc. Sodium nitrate ($NaNO_3$), potassium permanganate ($KMnO_4$), and sulfuric acid (H_2SO_4, 98%) were purchased from QReC Chemical Co., Ltd. Hydrogen peroxide (H_2O_2, 30 vol%) was provided by Samchun Pure Chemical Co., Ltd. Chloroform was supplied by RCL Labscan Limited. Polyethyleneimine (PEI, $M_w = 60\,000$ g mol^{-1}, 50 wt% aqueous solution) was purchased from Acros Organics, Thermo Fisher Scientific Inc. Polyurethane foam (PUF) was supplied by Bangkok Panel & Pipe Insulation Co., Ltd. All solutions were prepared using deionized (DI) water.

2.2 Preparation of FGO

GO was prepared using a modified Hummers' method.[46,47] To synthesize functionalized graphene oxide (FGO), a DOPO–GPTMS adduct was first prepared by adding 5.4 g of DOPO and 2.2 g of GPTMS into a three-necked flask containing 60 mL of chloroform. The mixture was vigorously stirred at 60 °C for 24 h to allow the reaction between DOPO and GPTMS to occur. After the reaction, the solvent was partially evaporated to reduce the volume to approximately 10 mL, yielding a concentrated DOPO-GPTMS solution. Separately, a GO dispersion was prepared by adding 2 g of GO into a mixed solvent consisting of 60 mL of deionized (DI) water and 240 mL of ethanol, followed by sonication for 1 h to obtain a homogeneous suspension. The prepared DOPO-GPTMS solution was then added to the GO dispersion, and the mixture was stirred at 80 °C for 24 h to allow the grafting reaction to occur. Finally, the resulting product was freeze-dried for 24 h to obtain the functionalized graphene oxide (FGO).

2.3 Preparation of coating dispersions

The flame-retardant dispersion was prepared by first dissolving polyethyleneimine (PEI) in deionized (DI) water to obtain a 0.7 wt% solution, which was stirred for 2 h at room temperature (RT). Subsequently, GO or FGO was added to the PEI solution at a concentration of 5 wt%. The resulting mixture was ultrasonicated for 1 h to obtain a homogeneous PEI/GO or PEI/FGO dispersion.

2.4 Preparation of coated samples

PUF samples were coated with flame-retardant dispersions to improve their fire resistance. Two coating systems were prepared for comparison: a PEI/GO dispersion and a PEI/FGO dispersion, as illustrated in Fig. 1. These two systems were designed to evaluate the effect of graphene oxide functionalization on the flame-retardant performance of PUF. The coatings were applied using a layer-by-layer (LbL) assembly process consisting of two deposition cycles. In each cycle, the PUF samples were immersed in the designated dispersion, dried at 70 °C for 4 h, and then cooled to room temperature (RT). The coating procedure was repeated once more to complete the second cycle, followed by a final drying step at 70 °C for 6 h. Using this method, three types of samples were obtained: PUF (uncoated control), PUF/GO (PUF coated with a 5 wt% GO dispersion), and PUF/FGO (PUF coated with a 5 wt% FGO dispersion).

2.5 Characterizations

The chemical interactions between DOPO, silane, and the GO surface were analyzed using Fourier-transform infrared spectroscopy (FTIR). Spectra were collected over the range of 600–4000 cm^{-1}. The spectra were recorded using a PerkinElmer Spectrum FTIR spectrometer in transmission mode with KBr pellets, at a resolution of 4 cm^{-1} with 32 scans. To analyze the gas composition of the thermal decomposition process, a thermogravimetric-infrared instrument (TGA; Mettler-Toledo, TGA/DSC 3+ and FT-IR; Bruker, INVENIO® S) was employed. The powder samples were heated from 35 °C to 700 °C at a heating rate of 10 °C min^{-1} under a nitrogen atmosphere. X-ray photoelectron spectroscopy (XPS) was performed using a PHI VersaProbe 4 spectrometer equipped with Al Kα radiation (1486.6 eV) to analyze the elemental composition and chemical states of GO and FGO. Sample preparation for XPS analysis was similar to that used for SEM. The samples were mounted on a sample holder using a carbon tape to ensure stable positioning in the XPS chamber. Prior to analysis, the samples were evacuated. X-ray diffraction (XRD) was used to determine the interlayer spacing of the GO sheets before and after functionalization using a Bruker D8 Advance X-ray diffractometer. The XRD patterns were recorded using Cu Kα radiation ($\lambda = 1.54$ Å) as the X-ray source. The diffraction angle (2θ) was scanned from 5° to 50° at a scanning rate of 20° min^{-1}. The synthesized FGO was further characterized by Raman spectroscopy using a HORIBA XploRA™ PLUS micro-Raman spectrometer equipped with a 532 nm laser excitation source. The morphologies of GO, FGO, and the resulting char residues were examined using scanning electron microscopy (SEM) coupled with energy-dispersive X-ray spectroscopy (EDS) (JEOL JMS-6400LV).

Thermogravimetric analysis (TGA) was performed using a METTLER TOLEDO TGA/DSC 3+ thermogravimetric analyzer. The samples were heated from room temperature to 800 °C at a heating rate of 10 °C min^{-1} under both air and nitrogen atmospheres.

The flame retardancy of the samples was evaluated using the UL-94 vertical burning test (ASTM D3801-19) with an ATLAS

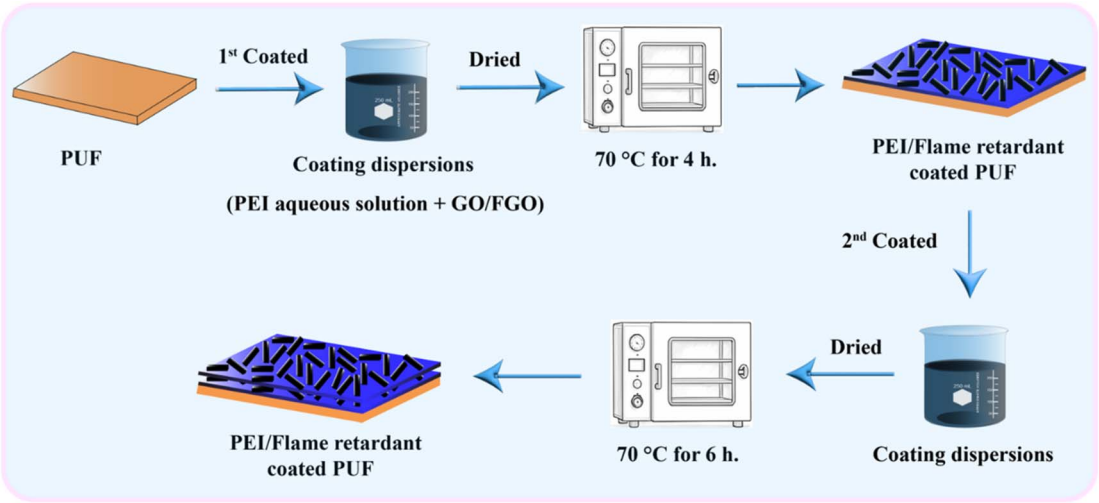

Fig. 1 Schematic illustration of the layer-by-layer assembly of PEI/flame-retardant coatings on the PUF surface.

HVUL-2 instrument. The limiting oxygen index (LOI) was measured using a Stanton Redcroft oxygen index instrument (Model PL) in accordance with ASTM D2863-06A. The specimen dimensions used for the LOI test were 110 × 6.5 × 3 mm^3.

The compressive strength of the samples (10 × 10 × 7 mm^3) was measured using an electromechanical universal testing machine (Tinius Olsen, 5ST) in accordance with ISO 1798 : 2008, at a compression rate of 5 mm min^{-1}. The compressive strength was defined as the compressive stress at 80% strain. The reported values represent the average of five specimens.

3 Results and discussion

3.1 Characterizations of GO/FGO structure

The FTIR spectra of GO and FGO are shown in Fig. 2. The absorption peak at 1730 cm^{-1} in the GO spectrum is attributed to the C=O stretching vibrations of carboxyl and carbonyl groups.[48] The sharp signal observed in the 1600–1650 cm^{-1} region is attributed to the skeletal vibration of sp^2 C=C bonds in the graphitic domains of graphene oxide.[28,49] The strong peak at 3420 cm^{-1} is due to the stretching vibrations of the O–H stretching vibration, indicating the presence of abundant hydroxyl groups on the GO surface.[49]

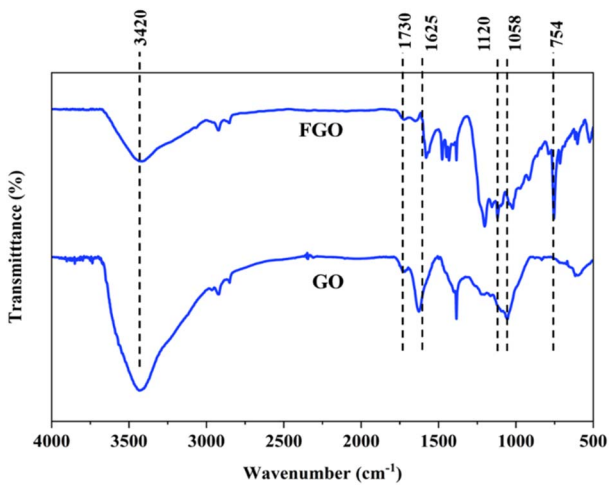

Fig. 2 FTIR spectra of GO and FGO.

After functionalization, several changes can be observed in the spectrum of FGO, indicating the successful modification of GO with the DOPO-GPTMS adduct. In particular, a new absorption peak at 754 cm^{-1} appears in the FGO spectrum, which can be attributed to the P–C stretching vibration, confirming the incorporation of DOPO into the GO structure through the reaction between the P–H groups of DOPO and the epoxy groups of GPTMS.[28] Moreover, the intensity of the O–H stretching band at 3420 cm^{-1} decreases in the FGO spectrum compared with that of GO, suggesting that part of the hydroxyl groups on GO participated in the grafting reaction with GPTMS. These spectral changes provide evidence for the successful functionalization of GO with the DOPO-GPTMS adduct. Furthermore, the absorption band at 1058 cm^{-1}, attributed to C–O stretching vibrations of oxygen-containing groups in GO, such as epoxy groups, shifts to approximately 1120 cm^{-1} after functionalization. This shift can be attributed to the hydrolysis and condensation reactions of GPTMS, where hydrolyzed silane groups react with oxygen-containing groups on the GO surface to form Si–O–C linkages, along with possible Si–O–Si bonds resulting from silanol self-condensation.[50] These results support the successful grafting of GPTMS onto the surface of GO sheets.

The chemical composition and bonding states of GO and its functionalized product were analyzed using X-ray photoelectron spectroscopy (XPS). The XPS survey spectra of GO and FGO are presented in Fig. 3a. The high-resolution C 1s spectrum (Fig. 3b) can be deconvoluted into three main components. The peak at 285.01 eV corresponds to C–C bonds, while the peak at 287.03 eV is attributed to C–O–C bonds. The peak observed at 288.56 eV is assigned to O–C=O groups, indicating the presence of oxygen-containing functional groups on the GO

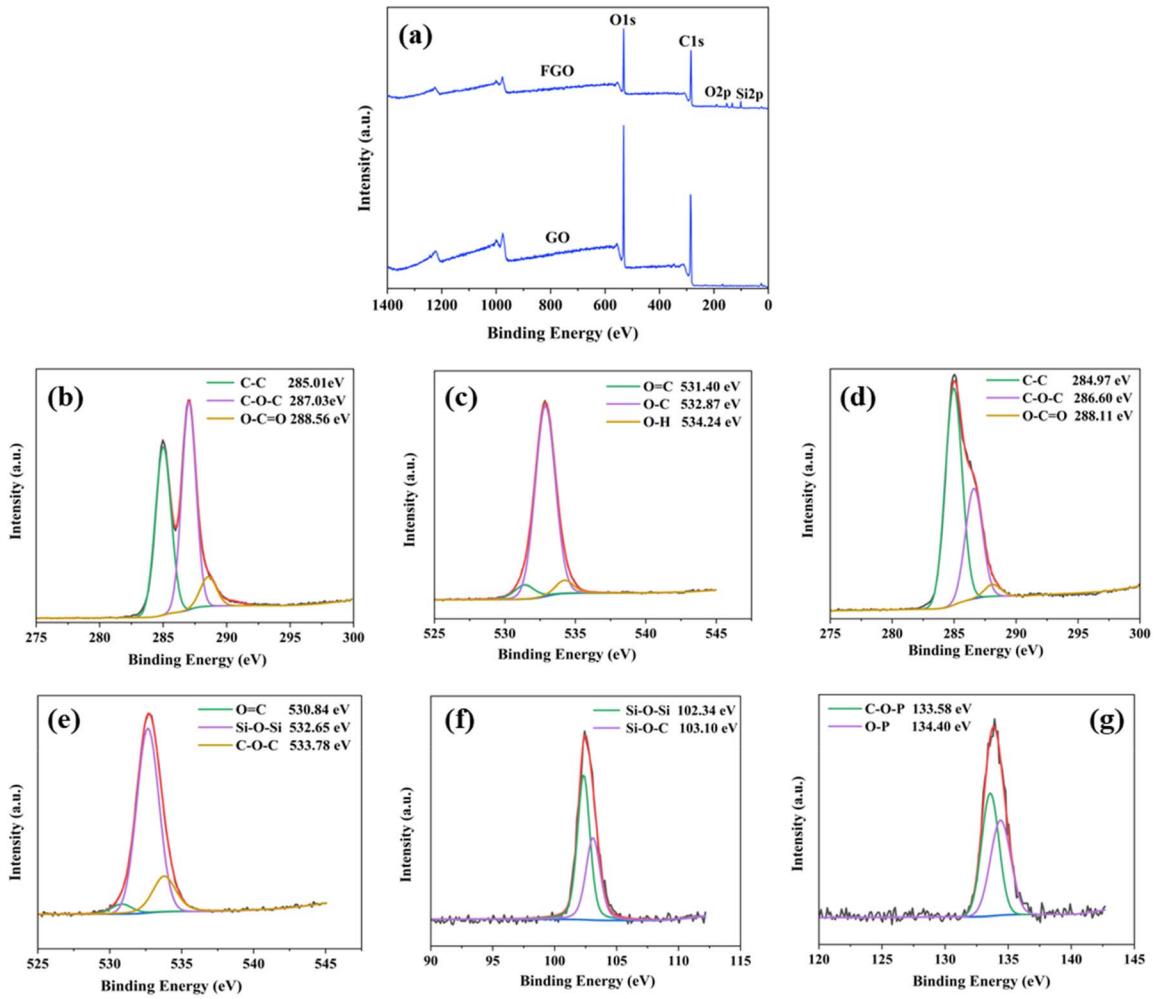

Fig. 3 XPS spectra of GO and FGO. (a) Wide scan survey spectra, (b) XPS C 1s spectrum of GO, (c) XPS O 1s of GO, (d) XPS C 1s of FGO, (e) XPS O 1s of FGO, (f) XPS Si 2p of FGO, and (g) XPS P 2s of FGO.

surface.[51,52] The high-resolution O 1s spectrum of GO, shown in Fig. 3c, can be fitted into three components located at 531.40, 532.87, and 534.24 eV, which are assigned to C═O (carbonyl), C–O (epoxy or hydroxyl), and O–H groups, respectively.[52,53] The high-resolution C 1s spectrum of FGO, shown in Fig. 3d, reveals notable changes compared with that of GO. The intensities of the C–O–C (286.60 eV) and O–C═O (288.11 eV) peaks decrease significantly, indicating that some oxygen-containing functional groups on GO participated in the reaction during the functionalization process.[51,52] Meanwhile, the O 1s spectrum of FGO (Fig. 3e) can be deconvoluted into three components located at 530.84, 532.65, and 533.78 eV, which are assigned to O═C, Si–O–Si, and C–O–C bonds, respectively.[28,53] The appearance of the Si–O–Si peak further confirms the successful grafting of GPTMS onto the GO sheets. Additionally, the Si 2p spectrum of FGO (Fig. 3f) can be deconvoluted into two peaks at 102.34 eV and 103.10 eV, corresponding to Si–O–Si and Si–O–C bonds, respectively.[28,51] Furthermore, the P 2p spectrum (Fig. 3g) exhibits two distinct peaks at 133.58 eV and 134.40 eV, which are assigned to C–O–P and O–P bonds, respectively.[54,55] These results confirm the successful introduction of the DOPO moiety and suggest the formation of covalent linkages between GO and the DOPO–GPTMS adduct.

X-ray diffraction (XRD) was used to investigate the changes in the interlayer spacing of GO and FGO. The interlayer spacing (d) was calculated using Bragg's equation, which states that $n\lambda = 2d \sin\theta$ (where $\lambda = 0.154$ nm and θ the measured diffraction angle). As shown in Fig. 4, GO exhibits a characteristic diffraction peak at $2\theta = 10.76°$, corresponding to an interlayer spacing of 0.82 nm. This value is significantly larger than that of graphite ($2\theta \approx 26.51°$, $d = 0.37$ nm) due to the presence of oxygen-containing functional groups and intercalated molecules between the GO layers.[50] After functionalization, the characteristic GO diffraction peak nearly disappears, and a broad diffraction feature appears around $2\theta \approx 26.5°$, which is close to the diffraction peak of graphite.[51] This change indicates the partial removal of oxygen-containing groups and the partial restacking of graphene layers during the functionalization process. The appearance of this broad peak, together with the disappearance of the GO peak, suggests that the DOPO–silane layer was successfully grafted onto the GO surface, altering the stacking structure of the graphene sheets.

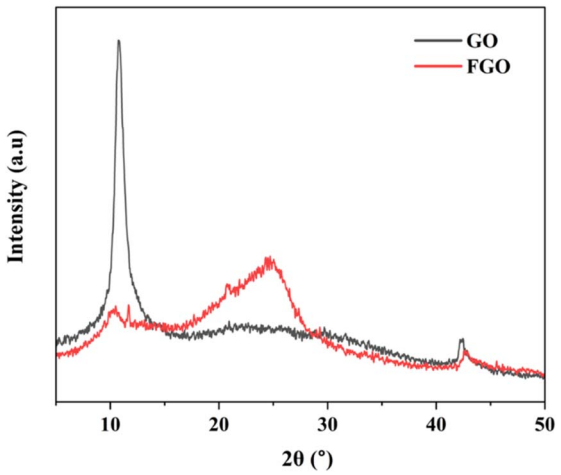

Fig. 4 XRD spectra of GO and FGO.

The Raman spectra of GO and FGO are shown in Fig. 5. Two prominent peaks are observed in the Raman spectrum of GO: the D band at 1348 cm^{-1} and the G band at 1573 cm^{-1}. The D band is associated with structural defects and the reduction of the in-plane sp^2 domain size, while the G band corresponds to the in-plane vibration of sp^2-bonded carbon atoms in the graphene lattice.[52,53] The degree of disorder and the number of defect sites in graphene-based materials can be evaluated using the intensity ratio of the D band to the G band (I_D/I_G), where a higher ratio indicates a higher level of defects.[51] As shown in Fig. 5, the I_D/I_G ratio increases from 0.89 for GO to 1.26 for FGO after functionalization with the silane cross-linker. This increase suggests the introduction of additional defect sites and the partial conversion of sp^2 carbon to sp^3 carbon, resulting from the covalent grafting of the DOPO–GPTMS adduct onto the GO surface. These results provide further evidence for the successful functionalization of GO.

3.2 Morphology of GO and FGO

The surface morphology and elemental composition of GO and FGO were analyzed using SEM coupled with energy-dispersive X-ray spectroscopy (SEM–EDS) to verify the success of the grafting process. As shown in Fig. 6a, the pristine GO sheets exhibit a relatively smooth and layered surface morphology. The corresponding EDS spectrum (Fig. 6b) reveals the presence of carbon (17.8 wt%) and oxygen (82.2 wt%), confirming the abundance of oxygen-containing functional groups on the GO surface. In contrast, the surface morphology of FGO (Fig. 6c) becomes noticeably rougher and more irregular, indicating the deposition of additional materials on the GO sheets after functionalization. This modification is further supported by the EDS analysis (Fig. 6d), which shows the presence of silicon (10.1 wt%) and phosphorus (15.9 wt%), along with carbon (17.7 wt%) and oxygen (56.3 wt%). The appearance of Si and P elements confirms the successful incorporation of the DOPO–GPTMS adduct onto the GO surface. In particular, the presence of silicon suggests the formation of siloxane structures resulting from the hydrolysis and condensation reactions of GPTMS during the grafting process.[48]

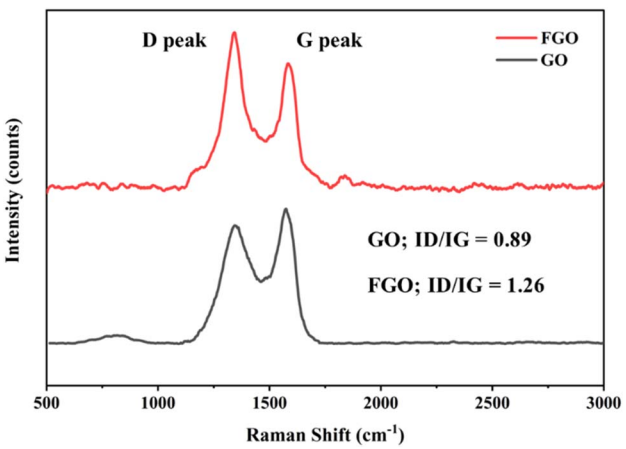

Fig. 5 Raman spectra of GO and FGO.

Multiple characterization techniques confirmed the successful synthesis of functionalized graphene oxide (FGO), as illustrated in Fig. 7. FTIR and XPS analyses verified the grafting of the DOPO–GPTMS adduct onto the GO surface through reactions between the hydrolyzed alkoxy groups of GPTMS and the oxygen-containing functional groups on GO. This process led to the formation of Si–O–C linkages between the silane and the GO surface, accompanied by the formation of Si–O–Si bonds through condensation reactions between silanol groups. Furthermore, XRD and Raman spectroscopy revealed structural changes in GO after functionalization, including disruption of the layered structure and an increase in defect sites, indicating the successful covalent modification of the GO surface and confirming the formation of FGO.

3.3 Thermal stability

The thermal stability of GO and FGO was evaluated by thermogravimetric analysis (TGA), and the corresponding TGA and DTG curves are shown in Fig. 8(a) and (b). GO exhibits two main stages of thermal degradation. The first stage occurs around 100 °C and corresponds to the evaporation of physically adsorbed water molecules on the hydrophilic GO surface. The second stage, occurring near 220 °C, is attributed to the rapid decomposition of oxygen-containing functional groups such as –OH and –COOH groups present on the GO sheets.[50,52] In contrast, FGO exhibits three degradation stages. The first stage between 30 °C and 120 °C is mainly associated with the evaporation of absorbed moisture. The second stage, occurring between 120 °C and 300 °C, corresponds to the removal of residual or weakly bound silane species. The extent of weight loss in this stage is noticeably smaller than that observed for GO, indicating that the grafted DOPO-GPTMS structure improves the thermal stability of the material. The third degradation stage, appearing around 300–350 °C, is attributed to the decomposition of the DOPO–GPTMS structures covalently grafted onto the GO sheets.[56] The DTG curves (Fig. 8b) further demonstrate that GO exhibits a sharp degradation peak around 220 °C, indicating rapid thermal decomposition of oxygen-containing groups. In comparison, FGO shows broader

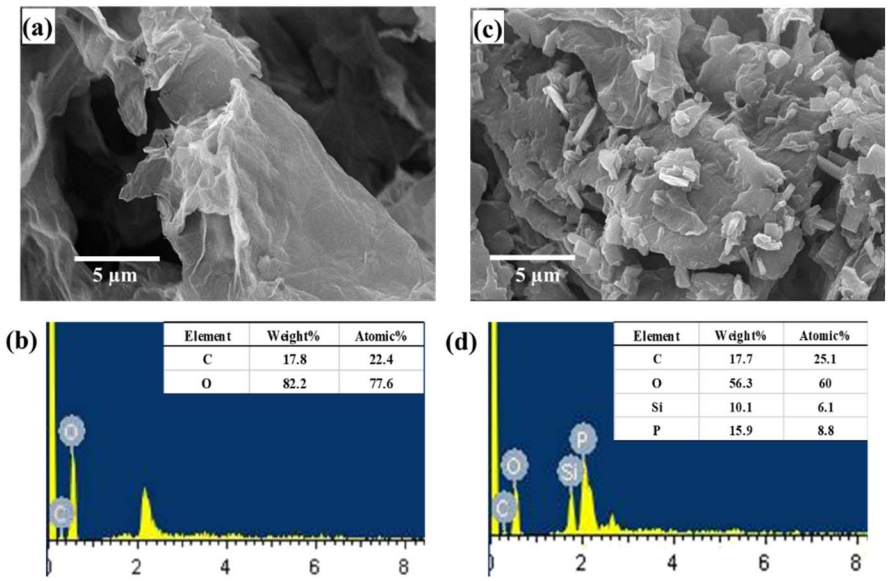

Fig. 6 SEM image (a) and EDS spectrum (b) of GO, alongside the SEM image, (c) and EDS spectrum (d) of FGO.

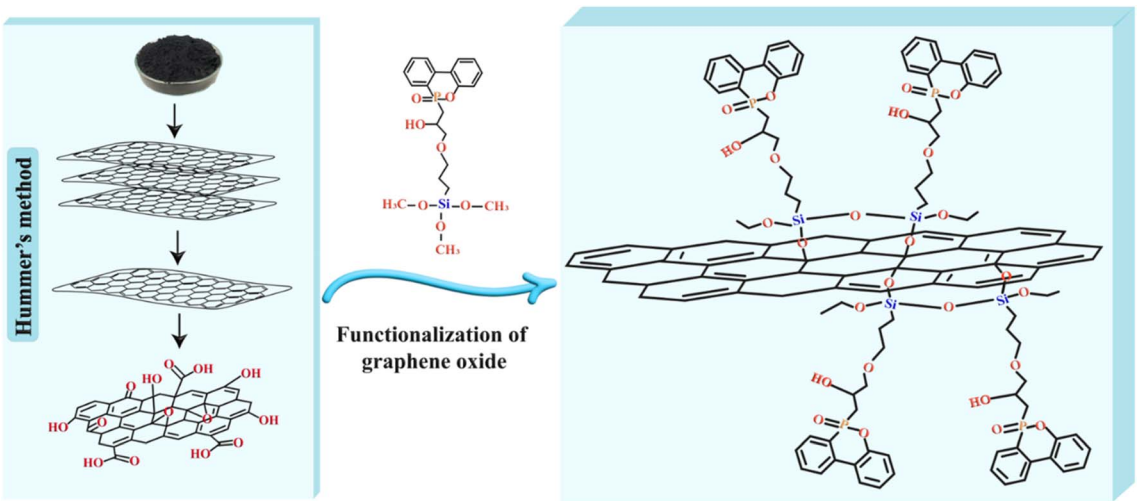

Fig. 7 The schematic diagram of the synthesis of FGO.

and less intense degradation peaks that shift toward higher temperatures, suggesting a slower degradation process after functionalization.

Moreover, the residual char yield of FGO at 700 °C (≈52%) is higher than that of GO (≈47%), indicating improved thermal stability after functionalization.[51] The enhanced thermal stability of FGO can be attributed to the formation of a phosphorus–silicon structure, where the siloxane network (Si–O–Si) formed by GPTMS provides high thermal resistance, while the phosphorus-containing DOPO groups promote char formation. These synergistic effects contribute to the improved thermal stability of FGO.

3.4 Flame retardancy performance

The effectiveness of the GO and FGO coatings in reducing the flammability of PUF was evaluated using the UL-94 vertical burning test, and the results are shown in Fig. 9. The uncoated control sample, neat PUF, ignited immediately and was completely consumed within 12 s (Fig. 9a), demonstrating its high flammability. Conversely, the PUF/GO sample exhibited slightly improved fire resistance (Fig. 9b). The GO coating, stabilized by electrostatic interactions between the positively charged PEI binder and the negatively charged functional groups on the GO surface, formed a protective layer that partially hindered heat transfer and oxygen diffusion during combustion. However, this barrier effect was limited, and the PUF/GO sample was still completely consumed after approximately 20 s, leaving little char residue. In contrast, the PUF/FGO sample exhibited significantly enhanced flame-retardant performance. Although the material ignited upon flame exposure, the flame self-extinguished immediately after removal of the ignition source, and the sample maintained its original

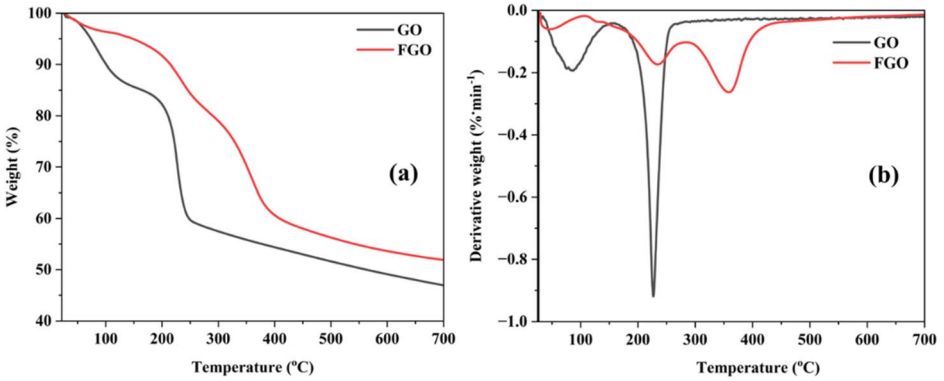

Fig. 8 TGA (a), DTG curves (b) of GO and FGO under nitrogen atmosphere.

shape without reignition (Fig. 9c). Consistent with this behavior, the PUF/FGO sample achieved the highest UL-94 classification (V-0), whereas neat PUF and PUF/GO failed to obtain any rating. The superior flame-retardant performance of PUF/FGO can be attributed to the synergistic effect of phosphorus and silicon elements introduced by the DOPO-GPTMS structure, together with the barrier effect of graphene sheets. These observations are consistent with the TGA results, which showed higher thermal stability and increased char yield for FGO compared with GO, further demonstrating the enhanced flame-retardant effectiveness of the FGO coating.

The flame resistance of the materials was further quantitatively evaluated using the Limiting Oxygen Index (LOI) test, and the results are summarized in Fig. 10. Neat PUF exhibited high flammability, with a low LOI value of 21.8%. Coating with 5 wt% GO moderately increased the LOI to 26.3%, indicating a slight improvement in flame resistance. By comparison, the PUF/FGO sample showed a significant increase in LOI to 34.2%, demonstrating substantially enhanced flame-retardant performance. These LOI results are consistent with the UL-94 burning behavior, further confirming the superior flame-retardant effectiveness of the FGO coating.

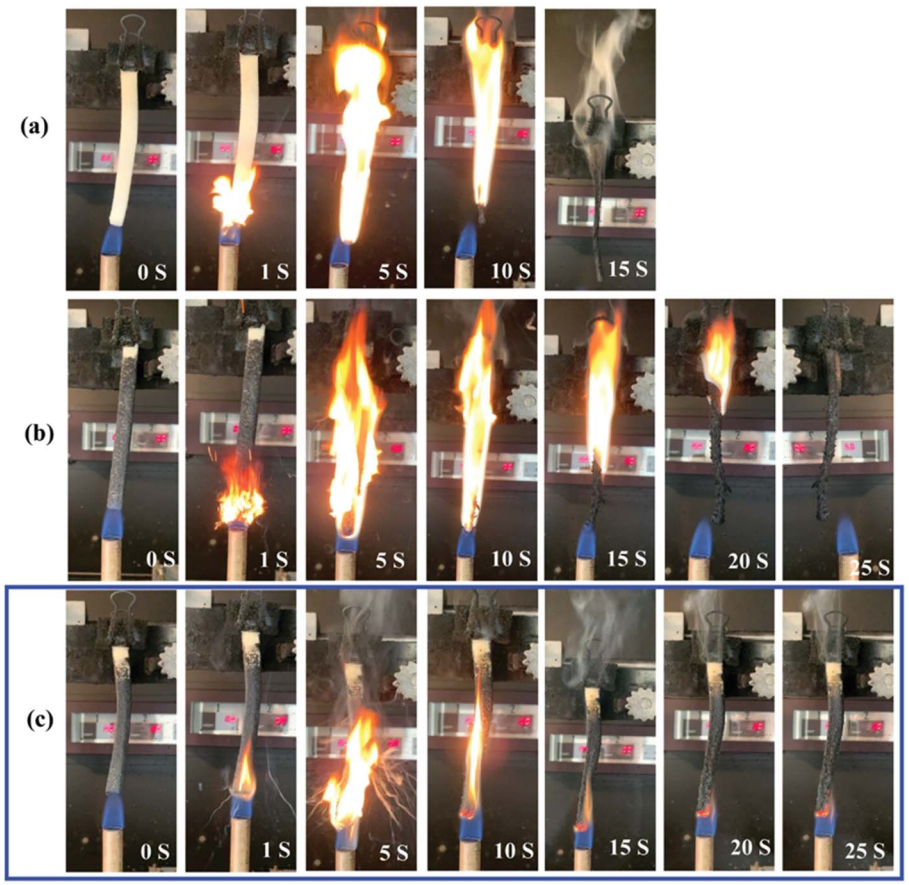

Fig. 9 Vertical burning of neat PUF (a), PUF/GO (b), and PUF/FGO (c).

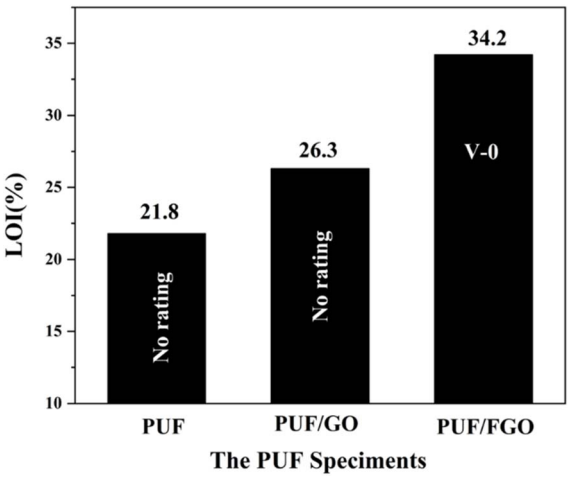

Fig. 10 LOI values and UL-94 vertical burning classifications of the PUF specimens.

To further elucidate the combustion behavior of the samples, the volatile decomposition products of neat PUF, PUF/GO, and PUF/FGO were monitored using real-time TGA–FTIR analysis. As shown in Fig. 11, the total absorbance intensity of the evolved gaseous species from neat PUF was significantly higher than that from the coated samples, indicating a considerable reduction in volatile release during the thermal decomposition of PUF/FGO. The major pyrolysis gases of neat PUF were identified as CO_2, CH_4, and H_2O (Fig. 11a), corresponding to the stretching vibration of C=O at 2240–2400 cm^{-1}, the symmetric and asymmetric stretching vibrations of C–H at 2750–3000 cm^{-1}, and the combined aromatic ring and –OH stretching vibrations in the ranges of 1300–1900 cm^{-1} and 3500–4000 cm^{-1}, respectively.[57] Compared with neat PUF, the intensities of these absorption bands were markedly reduced for PUF/FGO (Fig. 11c), suggesting that a larger fraction of carbon remained in the condensed phase to form a stable char layer rather than being released as volatile combustible gases. Notably, the maximum absorbance intensity of CO_2 for PUF/FGO decreased by approximately 46% relative to neat PUF (Fig. 11c and d), indicating a significant suppression of volatile fuel evolution during thermal degradation. Since the heat release during combustion is closely related to the amount of combustible gases reaching the flame zone, the reduced gas evolution observed for PUF/FGO suggests a potential decrease in heat release intensity.[58,59]

Furthermore, the overall gas evolution of PUF/FGO was substantially lower than that of neat PUF and PUF/GO, while thermogravimetric analysis revealed a significantly higher char residue of approximately 52%. This result indicates that the functionalized graphene effectively promotes carbon retention in the condensed phase, forming a protective barrier layer. The formation of this dense char layer restricts heat and mass transfer, thereby suppressing the release of flammable volatiles and reducing smoke generation. Consequently, the incorporation of FGO provides a strong barrier effect, significantly mitigating both thermal hazards and smoke production during PUF combustion.

3.5 Char analysis

To better understand the flame-retardant mechanism, the morphology of the coating layers and the char residues was analyzed using SEM, as shown in Fig. 12. Fig. 12a presents the cross-sectional images of the PUF/GO and PUF/FGO samples before combustion. It can be observed that the average thickness of the flame-retardant coating layer is approximately 200 ±

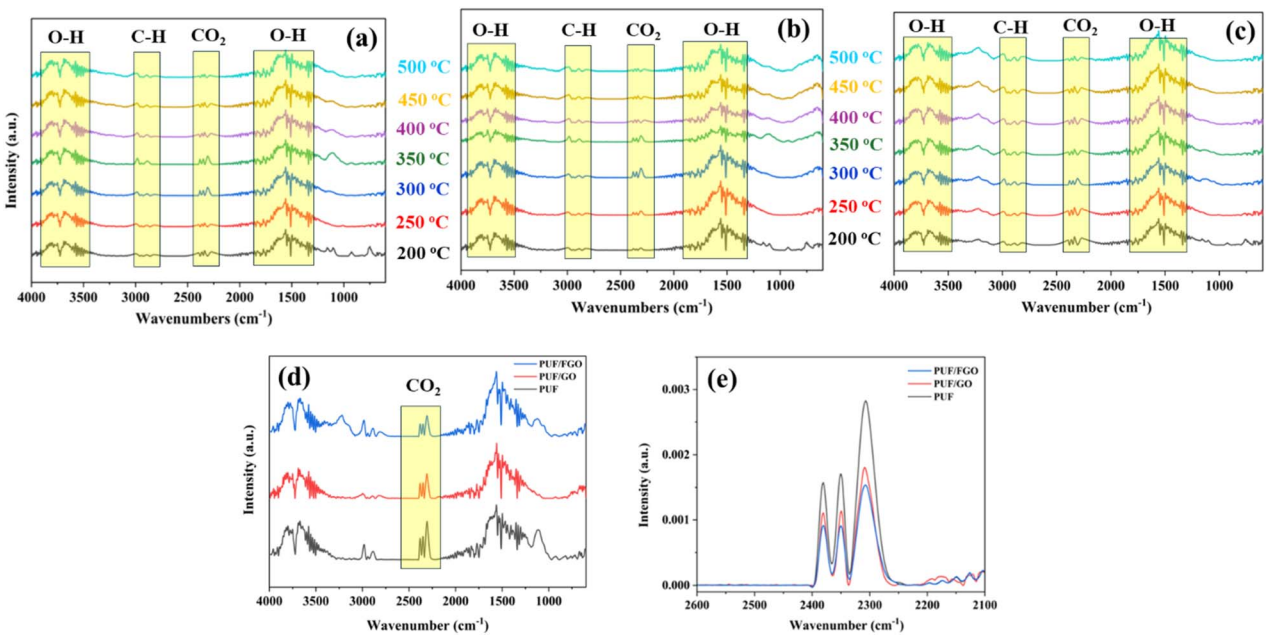

Fig. 11 TGA–FTIR spectra of gaseous decomposition products for (a) PUF, (b) PUF/GO, and (c) PUF/FGO; (d) spectra at the temperature of maximum thermal degradation; and (e) absorbance intensity in the CO_2 region derived from (d).

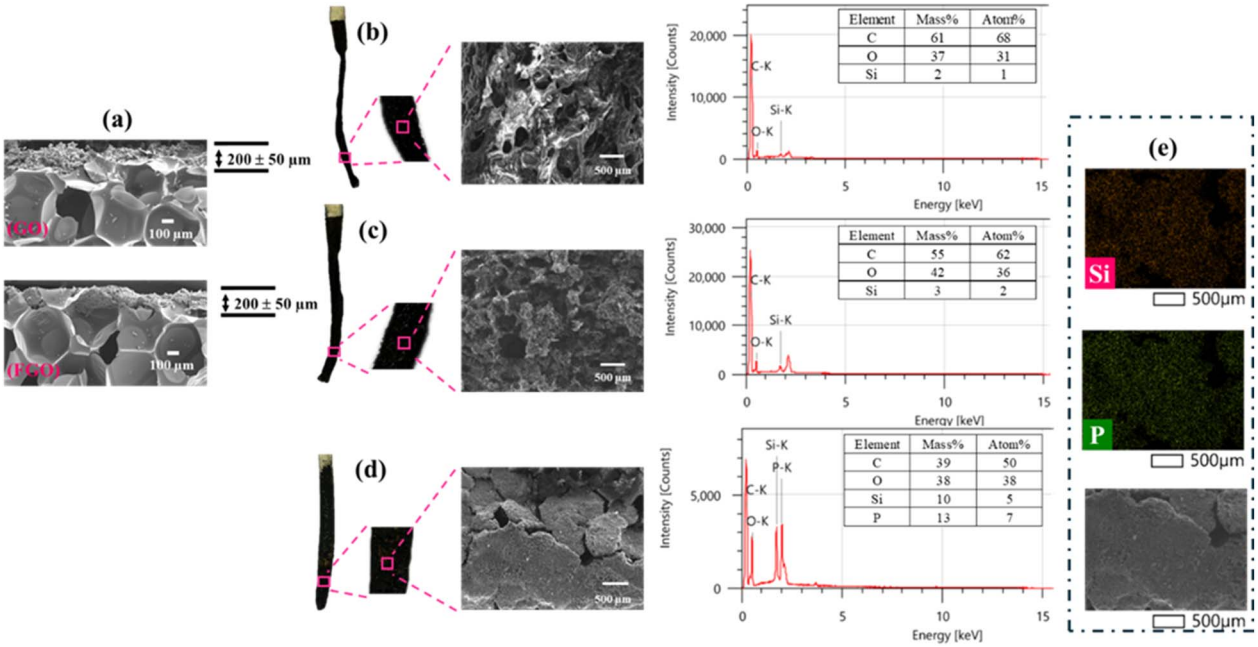

Fig. 12 Cross-sectional SEM images of PUF/GO and PUF/FGO (a). SEM images and EDX spectra of residual char after burning neat PFU (b), PUF/GO (c), PUF/FGO (d), and EDX elemental mapping of Si and P (e).

50 μm for both samples. However, the FGO coating forms a denser and more compact protective layer compared with the GO coating, indicating a more uniform and tightly packed coating structure. After combustion, the morphology of the char residues was further examined. The neat PUF sample was almost completely consumed by the flame, leaving nearly no char residue due to its inherent flammability (Fig. 12b). In comparison, the PUF/GO sample formed a char layer; however, the residue was thin, porous, and lacked structural integrity. Large holes were observed on its surface (Fig. 12c), which could allow oxygen and volatile combustible gases to penetrate, thereby accelerating the combustion of the underlying polymer.[60] In contrast, the PUF/FGO sample generated a thick, compact, and continuous char layer (Fig. 12d). This robust structure effectively insulated the polymer substrate and suppressed heat and mass transfer during combustion, thereby enhancing flame resistance and maintaining the structural integrity of the material.[43] EDS analysis and elemental mapping of the char residues provided further insight into the flame-retardant mechanism. While the char residues from neat PUF and PUF/GO contained negligible amounts of phosphorus (P) and silicon (Si), the PUF/FGO char was enriched with both elements. Moreover, elemental mapping (Fig. 12e) revealed that P and Si were uniformly distributed throughout the FGO char residue. This homogeneous distribution suggests the formation of a stable phosphosilicate network during combustion. Such a network contributes to the development of a dense and compact protective char layer, which is significantly more robust than that formed by GO alone. The formation of this ceramic-like barrier helps explain the higher char yield observed in the TGA analysis and is consistent with the improved LOI and UL-94 flame-retardant performance.

3.6 Flame-retardant mechanism

Based on the experimental results, the flame-retardant mechanism of FGO in PUF can be proposed, as illustrated in Fig. 13, which primarily operates in the condensed phase. During combustion, the graphene sheets in the coating act as an effective physical barrier, promoting the formation of a stable char layer on the polymer surface. This protective layer insulates the underlying material, thereby reducing the heat release rate and suppressing the emission of flammable gases and smoke.[61] During thermal decomposition, DOPO in FGO generates phosphorus-rich species, which facilitate char formation and contribute to the development of a protective carbonaceous residue. In addition, phosphorus-containing radicals can scavenge hydrogen radicals in the flame, thereby interrupting the combustion chain reactions.[48,62,63] Meanwhile, GPTMS forms a thermally stable Si–O–Si network, which promotes the formation of a graphitized char structure and further enhances the thermal stability of the condensed-phase residue.[64] In addition, the nitrogen-containing PEI binder releases nonflammable gases such as ammonia and water vapor during combustion, which dilute combustible gases and oxygen in the flame zone, providing an additional gas-phase flame-retardant effect.[44] As a result, the combined presence of phosphorus, silicon, and graphene forms a synergistic ternary system that significantly improves the fire resistance of the foam. This synergistic effect delays ignition, promotes the formation of a stable protective char layer, and effectively suppresses the transfer of heat and oxygen to the underlying PUF during combustion.

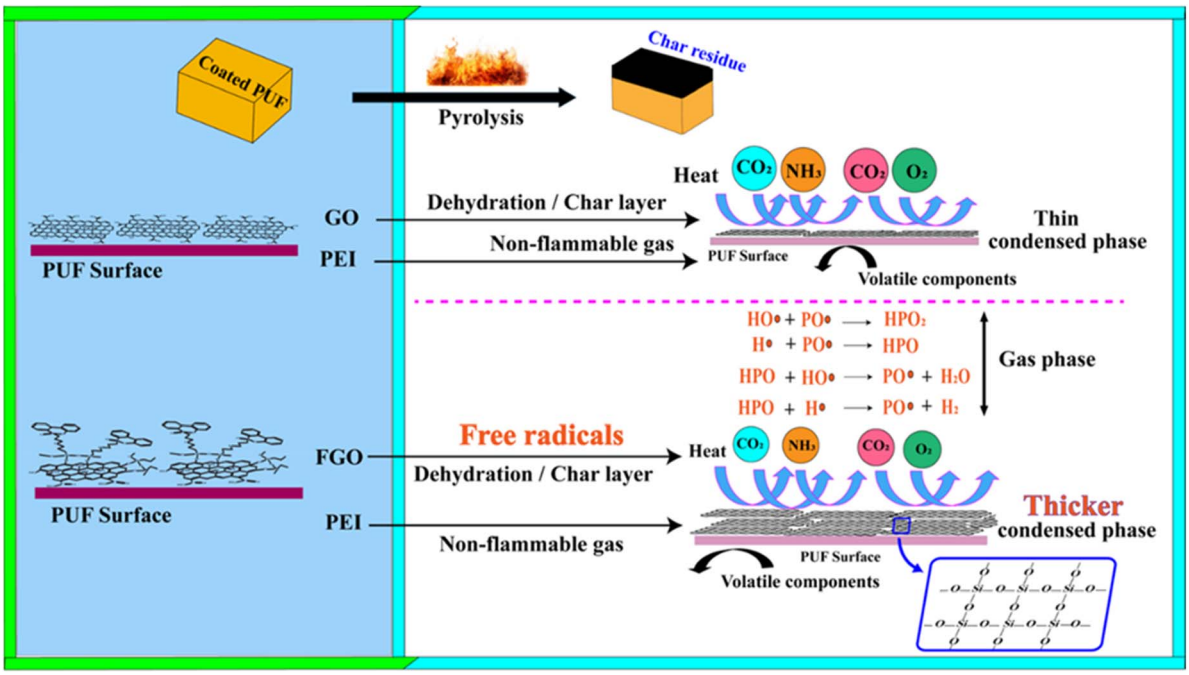

Fig. 13 Schematic of the flame-retardant mechanism of PUF/GO and PUF/FGO.

3.7 Mechanical properties and density

The coating process led to an observable increase in foam density. Specifically, the density of neat PUF was 0.0540 g cm^{-3}, whereas those of PUF/GO and PUF/FGO rose to 0.0708 g cm^{-3} and 0.0712 g cm^{-3}, representing increments of approximately 31% and 33%, respectively. This densification confirms the successful deposition of the graphene oxide-based flame-retardant system within the porous architecture of the foam. The influence of these coatings on the mechanical properties is depicted in Fig. 14. Despite the moderate density increase, the coated foams exhibited a remarkable enhancement in mechanical performance. The compressive strength of neat PUF was 0.53 MPa, while the PUF/GO and PUF/FGO composites reached 0.85 MPa and 1.34 MPa, respectively-marking substantial improvements of 60% and 152% over the pristine foam. Notably, the treatment did not compromise the inherent mechanical integrity of the substrate. This reinforcement is attributed to the infiltration of the flame-retardant/binder system into the surface micropores and structural defects, which effectively bridges weak points and enhances the structural compactness of the PUF. The presence of graphene oxide derivatives within the cellular framework reinforces the foam structure, thereby contributing to the enhanced compressive strength of the coated PUFs.

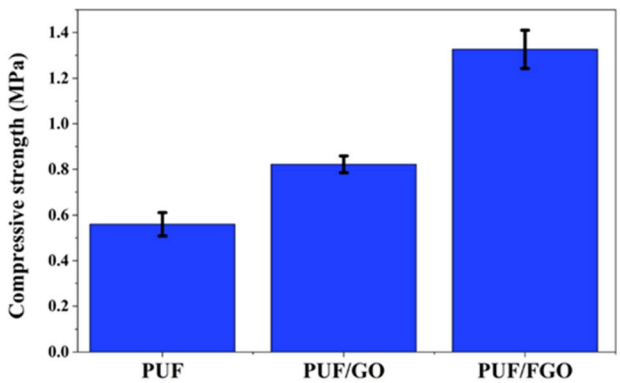

Fig. 14 Compressive strength of PUF, PUF/GO, and PUF/FGO.

4 Conclusions

This study successfully developed a novel functionalized graphene oxide (FGO: DOPO-GPTMS-GO) as a high-performance flame retardant, with its structure confirmed through comprehensive characterization including FTIR, XRD, Raman, and SEM-EDS. When applied to polyurethane foam (PUF) *via* a layer-by-layer coating process, the PUF/FGO composite exhibited outstanding flame retardancy, achieving a high LOI of 34.2% and a V-0 rating in UL-94 tests, significantly outperforming both neat PUF and PUF/GO. Real-time TG-FTIR analysis further elucidated the combustion behavior, revealing a 46% reduction in CO_2 evolution and a substantial char yield of 52%, which indicates that the FGO effectively suppresses heat and smoke hazards by sequestering volatile fragments into the condensed phase. This synergistic mechanism is driven by the formation of a dense, continuous phosphosilicate layer that acts as a physical shield, preventing further thermo-oxidative degradation. Beyond fire safety, the coating treatment remarkably enhanced the mechanical integrity of the foam, yielding a 152% increase in compressive strength (1.34 MPa) due to the effective infiltration of the FGO into structural defects and its role as a reinforcing backbone within the cellular framework. Consequently,

this work demonstrates a promising strategy for designing multifunctional, graphene-based flame retardants that simultaneously optimize the fire safety and mechanical performance of combustible polymer material.

Author contributions

Taweesak Boonsod: conceptualization, data curation, formal analysis, investigation, methodology, resources, writing – original draft. Qamber Ali: writing – review & editing, investigation. Wirunya Keawwattana and Kanoktip Boonkerd: conceptualization, project administration, funding acquisition, supervision, validation, writing – review & editing.

Conflicts of interest

The authors declare no conflicts of interest.

Data availability

All the data for the manuscript is available in the manuscript.

Acknowledgements

This work was supported by a PhD scholarship from Kasetsart University and International SciKU Branding (ISB), Faculty of Science, Kasetsart University. Authors wish to thank the Hub of Talents in Natural Rubber and the National Research Council of Thailand for the publication support. Partial support was also provided by the International Science & Technology Cooperation Program of Hainan Province (No. GHYF2025018). The authors are grateful to the Department of Materials Science, Faculty of Science, Chulalongkorn University, for providing the research facilities used in this project.

References

1 A. Kausar, *Polym.-Plast. Technol. Eng.*, 2017, **57**, 346–369.
2 Y. Jiang, H. Yang, X. Lin, S. Xiang, X. Feng and C. Wan, *Materials*, 2023, **16**, 2728.
3 A. Muhammed Raji, H. U. Hambali, Z. I. Khan, Z. Binti Mohamad, H. Azman and R. Ogabi, *J. Cell. Plast.*, 2022, **59**, 65–122.
4 Q. Wu, J. Zhang, S. Wang, B. Chen, Y. Feng, Y. Pei, Y. Yan, L. Tang, H. Qiu and L. Wu, *Front. Chem. Sci. Eng.*, 2020, **15**, 969–983.
5 J. Wang, C. Zhang, Y. Deng and P. Zhang, *Polymers*, 2022, **14**, 4586.
6 E. Singh and H. S. Nalwa, *J. Nanosci. Nanotechnol.*, 2015, **15**, 6237–6278.
7 J. Jaidev and S. Ramaprabhu, *J. Mater. Chem.*, 2012, **22**, 18775–18783.
8 M. Taş, Z. İşlek Cin, E. D. Sam Parmak and A. Çelik Bedeloğlu, *Polym. Compos.*, 2016, **39**, 1771–1778.
9 C. M. Santos, J. Mangadlao, F. Ahmed, A. Leon, R. C. Advincula and D. F. Rodrigues, *Nanotechnology*, 2012, **23**, 395101.
10 B. Yang, Y. Wang, L. Xiao, X. Hu and G. Zhou, *Macromol. Res.*, 2016, **25**, 21–26.
11 W.-Z. Fang, L. Peng, Y.-J. Liu, F. Wang, Z. Xu and C. Gao, *Chin. J. Polym. Sci.*, 2020, **39**, 267–308.
12 B. Sang, Z.-w. Li, X.-h. Li, L.-g. Yu and Z.-j. Zhang, *J. Mater. Sci.*, 2016, **51**, 8271–8295.
13 N. F. Attia, S. E. A. Elashery, A. M. Zakria, A. S. Eltaweil and H. Oh, *Mater. Sci. Eng. B*, 2021, **274**, 115460.
14 A. Kausar, I. Ahmad, M. H. Eisa and M. Maaza, *J. Carb. Res.*, 2023, **9**, 29.
15 J. Deng, P. Zhang, T. Jin, H. Zhou and J. Cheng, *RSC Adv.*, 2017, **7**, 54475–54484.
16 J. Jing, Y. Zhang, X. Tang, X. Li, M. Peng and Z. Fang, *RSC Adv.*, 2018, **8**, 4304–4313.
17 G. Yuan, B. Yang, Y. Chen and Y. Jia, *RSC Adv.*, 2018, **8**, 36286–36297.
18 Y. Sui, L. Qu, P. Li, X. Dai, Q. Fang, C. Zhang and Y. Wang, *RSC Adv.*, 2020, **10**, 13949–13959.
19 B. Wang, J. Liu, S. Yue, X. Wang, Y. Zhang, Y. Fu, T. Li and T. Wang, *J. Mater. Res. Technol.*, 2021, **13**, 2433–2441.
20 K. Dai, S. Sun, W. Xu, Y. Song, Z. Deng and X. Qian, *RSC Adv.*, 2018, **8**, 24993–25000.
21 P. The Long, N. Thi Ngoan, V. Thi Hoang Anh, N. Huu Dat, N. Vu Giang, Y. N. T. Thi and L. Nhu Hai, *RSC Adv.*, 2025, **15**, 43085–43094.
22 J. Vasiljević, I. Jerman, G. Jakša, J. Alongi, G. Malucelli, M. Zorko, B. Tomšič and B. Simončič, *Cellulose*, 2015, **22**, 1893–1910.
23 K. Liu, Y. Li, L. Tao and R. Xiao, *RSC Adv.*, 2018, **8**, 9261–9271.
24 H. Wang, S. Wang, X. Du, H. Wang, X. Cheng and Z. Du, *RSC Adv.*, 2019, **9**, 7411–7419.
25 W. Xie, S. Huang, D. Tang, S. Liu and J. Zhao, *RSC Adv.*, 2020, **10**, 1956–1965.
26 L. Cai, F. Xin, C. Zhai, Y. Chen, B. Xu and X. Li, *RSC Adv.*, 2021, **11**, 6781–6790.
27 H. Wang, S. Wang, X. Du, H. Wang, X. Cheng and Z. Du, *RSC Adv.*, 2019, **9**, 7411–7419.
28 F. Qi, M. Tang, N. Wang, N. Liu, X. Chen, Z. Zhang, K. Zhang and X. Lu, *RSC Adv.*, 2017, **7**, 31696–31706.
29 T. Liu, F. Wang, G. Li, P. Liu, C. Gao, Y. Ding, S. Zhang, X. Kong and M. Yang, *J. Appl. Polym. Sci.*, 2020, **138**, 49607.
30 C.-S. Wu, Y.-L. Liu, Y.-S. Chiu and W.-H. Ho, *J. Polym. Sci., Part A: Polym. Chem.*, 2003, **41**, 2354–2367.
31 S. Chernyy, S. Ulah, G. Sørensen, S. W. Tordrup, P. B. Pedersen and K. Almdal, *J. Appl. Polym. Sci.*, 2015, **132**, 41955.
32 C. Y. K. Lung and J. P. Matinlinna, *Dent. Mater.*, 2012, **28**, 467–477.
33 X. Chen, Y. Hu, C. Jiao and L. Song, *Polym. Degrad. Stab.*, 2007, **92**, 1141–1150.
34 Y. Xie, C. A. S. Hill, Z. Xiao, H. Militz and C. Mai, *Compos. Appl. Sci. Manuf.*, 2010, **41**, 806–819.
35 X. Qiu, Z. Li, X. Li and Z. Zhang, *Chem. Eng. J.*, 2018, **334**, 108–122.
36 Q. Liu, S. Gao, Y. Zhao, W. Tao, X. Yu and M. Zhi, *J. Mater. Sci.*, 2021, **56**, 9605–9643.

37 M. A. Ghriga, B. Grassl, M. Gareche, M. Khodja, S. E. I. Lebouachera, N. Andreu and N. Drouiche, *Polym. Bull.*, 2019, **76**, 6001–6029.
38 F. Meng, S. Kwon, J. Wang and Y. Yeo, in *Biomaterials for Cancer Therapeutics*, 2020, pp. 53–94, DOI: 10.1016/b978-0-08-102983-1.00003-x.
39 S. Saidin, M. A. Jumat, N. A. A. Mohd Amin and A. S. Saleh Al-Hammadi, *Mater. Sci. Eng. C*, 2021, **118**, 111382.
40 H. Pan, B. Yu, W. Wang, Y. Pan, L. Song and Y. Hu, *RSC Adv.*, 2016, **6**, 114304–114312.
41 H. Pan, Y. Lu, L. Song, X. Zhang and Y. Hu, *RSC Adv.*, 2016, **6**, 78286–78295.
42 X. Shi, P. Yang, X. Peng, C. Huang, Q. Qian, B. Wang, J. He, X. Liu, Y. Li and T. Kuang, *Polymer*, 2019, **170**, 65–75.
43 X. Qiu, C. K. Kundu, Z. Li, X. Li and Z. Zhang, *J. Mater. Sci.*, 2019, **54**, 13848–13862.
44 M. Guan, J. Li, Y. Fang, K. Dai, X. Liu and G. Tang, *J. Appl. Polym. Sci.*, 2024, **142**, e56535.
45 B. Palen, T. J. Kolibaba, J. T. Brehm, R. Shen, Y. Quan, Q. Wang and J. C. Grunlan, *ACS Omega*, 2021, **6**, 8016–8020.
46 M. Bera, P. Gupta and P. K. Maji, *J. Nanosci. Nanotechnol.*, 2018, **18**, 902–912.
47 A. M. D. Tour, *Dimiev.Tour*, 2014, **8**, 3060–3068.
48 M. Zhi, Q. Liu, H. Chen, X. Chen, S. Feng and Y. He, *ACS Omega*, 2019, **4**, 10975–10984.
49 K. Rhili, S. Chergui, A. S. ElDouhaibi and M. Siaj, *ACS Omega*, 2021, **6**, 6252–6260.
50 M. Gao, J. Li and X. Zhou, *Polym. Compos.*, 2018, **40**, E1274–E1282.
51 W. Wu, Y. Xu, H. Wu, J. Chen, M. Li, T. Chen, J. Hong and L. Dai, *J. Appl. Polym. Sci.*, 2019, **137**, 47710.
52 S. S. Abbas, G. J. Rees, N. L. Kelly, C. E. J. Dancer, J. V. Hanna and T. McNally, *Nanoscale*, 2018, **10**, 16231–16242.
53 Y. Chen, Y. W. Liu, Y. Xie, H. H. Zhang and Z. Zhang, *Surf. Coat. Technol.*, 2021, **423**, 127622.
54 H. Zhang, H. Wang, T. Wang, S. Han, X. Zhang, J. Wang and G. Sun, *ACS Appl. Polym. Mater.*, 2024, **6**, 1878–1890.
55 A. S. Singh, J. H. Advani and A. V. Biradar, *Dalton Trans.*, 2020, **49**, 7210–7217.
56 K. M. Aujara, B. W. Chieng, N. A. Ibrahim, N. Zainuddin and C. Thevy Ratnam, *Int. J. Mol. Sci.*, 2019, **20**, 1910.
57 L. Xu, J. Ma, J. Guo, Y. Li, S. Tan, H. Wang, L. Li and Z. Li, *J. Appl. Polym. Sci.*, 2024, **141**, e56229.
58 Y. Huang, Z. Zheng, C. Chen, C. Guo, X. Wang, Q. Zhou and D. Tu, *Eur. J. Wood Wood Prod.*, 2024, **82**, 731–745.
59 Q. Fu, L. Medina, Y. Li, F. Carosio, A. Hajian and L. A. Berglund, *ACS Appl. Mater. Interfaces*, 2017, **9**, 36154–36163.
60 H. Xin, Y. Chen, X. Li, Y. Li, Q. Peng and H. Luo, *Polym. Test.*, 2023, **128**, 108219.
61 L. Li, X. Shao, Z. Zhao, X. Liu, L. Jiang, K. Huang and S. Zhao, *ACS Omega*, 2020, **5**, 799–807.
62 W. Yan, J. Yu, M. Zhang, S. Qin, T. Wang, W. Huang and L. Long, *RSC Adv.*, 2017, **7**, 46236–46245.
63 N. H. Thi, H. T. Nguyen, D. L. Tran, H. T. Oanh, T. D. Doan, G. Le Nhat Thuy, H. Tran Nguyen, T. Van Nguyen and M. H. Hoang, *RSC Adv.*, 2025, **15**, 47587–47600.
64 G. Yuan, B. Yang, Y. Chen and Y. Jia, *Compos. Appl. Sci. Manuf.*, 2019, **117**, 345–356.